

Selective photoinduced antibacterial activity of amoxicillin coated gold nanoparticles. From one-step synthesis to *in vivo* cytocompatibility

M. Jazmín Silvero C.^{a,b}, D. M. Rocca^b, E. Artur de la Villarmois^c; Kelsey Fournier^a; Anabel E. Lanterna^a; M. F. Pérez^c; M. C. Becerra^{b*} and Juan C. Scaiano^{a*}.

^a Department of Chemistry and Biomolecular Sciences and Centre for Advanced Materials Research (CAMaR), University of Ottawa, 10 Marie Curie, Ottawa, Ontario K1N 6N5, Canada.

^b Instituto Multidisciplinario de Biología Vegetal (IMBIV-CONICET), Departamento de Ciencias Farmacéuticas and

^c Instituto de Farmacología Experimental Córdoba (IFEC-CONICET), Departamento de Farmacología. Facultad de Ciencias Químicas, Universidad Nacional de Córdoba. Haya de la Torre S/N. Córdoba X5000, Argentina.

† Corresponding Authors: *titoscaiano@mac.com; *becerra@fcq.unc.edu.ar

KEYWORDS: Antibiotic-Resistant, Nanoparticle, Bacteria, Light, Biodistribution, Cytocompatibility

ABSTRACT: Photoinduced antibacterial gold nanoparticles were developed as an alternative for the treatment of antibiotic resistant bacteria. Thanks to the amoxicillin coating, they possess high *in vivo* stability, selectivity for the bacteria wall, a good renal clearance, and are completely non-toxic for eukaryotic cells at the bactericidal concentrations. A simple one-step synthesis of amoxi@AuNP is described at mild temperatures using the antibiotic as both reducing and stabilizing agent. Time-resolved fluorescence microscopy proved these novel nano photosensitizers, with improved selectivity, are bactericidal but showing excellent biocompatibility toward eukaryotic cells at the same dose (1.5 µg/mL) when co-cultures are analyzed. Their stability in biological media, hemocompatibility and photo-antibacterial effect against sensitive and antibiotic resistant *Staphylococcus aureus* were evaluated *in vitro*, while toxicity, renal clearance and biodistribution were studied *in vivo* in male Wistar rats. The use of these nanoparticles to treat antibiotic-resistant infections is promising given their high stability and cytocompatibility.

1 Introduction

Antibiotic resistant (AR) bacteria and the lethal infections they can cause are a subject of public concern.^{1,2} Indeed, the World Health Organisation (WHO) has described AR as “a problem so serious that it threatens the achievements of modern medicine”.³ Thus, there is an urgent need for the development of novel strategies and drugs. In recent years, nanoparticles have been tested as potential antibacterial agents; particularly, gold nanoparticles (AuNPs) were chosen to act as photosensitizers because of their inert nature and effectiveness in spite of their polymorphism and polydispersity.⁴ Further, AuNPs plasmons can absorb visible light,⁵ thus avoiding the use of highly energetic wavelengths that cause cell photodamage, proving useful for cancer treatment.⁶ Additionally, we have shown the photoinduced bactericidal properties of AuNPs utilizing green light, even on AR clinical strains.⁷⁻¹⁰ Thus, plasmon excitation of the AuNPs can produce highly reactive oxygen species (ROS) levels causing oxidative stress after 4 hours of Photodynamic Antimicrobial Chemotherapy (PACT), leading to bacterial death. Furthermore, *in vitro* studies suggest that these AuNPs are non-toxic for eukaryotic cells. These results stimulated the present work to explore the selectivity towards prokaryotic cells in cell co-cultures and the biocompatibility and distribution of the particles *in vivo*.

Many *in vivo* studies on the biodistribution and toxic effects of AuNPs show that they are controlled by the nanomaterial size, shape and coating.¹¹⁻¹³ The limited pore size of the endothelial wall in the tissue is the primary delivery barrier for nanoparticles but also allows selective accumulation in

certain tissues. When nanoparticles are administered through intraperitoneal (IP) or intravenous injection, a variety of serum proteins bind to their surface, which are recognized, internalized and carried to the liver or spleen.¹⁴ It is known that the majority of the AuNPs after IP injection are distributed to the liver and spleen in 2-3 hours,¹⁵ and that AuNPs had a fast blood clearance rate being mostly distributed in the liver, followed by the spleen and lungs.¹⁶ No matter the pathway used, AuNPs seemed to migrate into the circulatory system first, and subsequently distributed into tissues and organs; thus, mainly distributed by passive targeting.¹⁷

It has been demonstrated that AuNPs can enhance their bactericidal properties when combined with antibiotics, such as vancomycin, aminoglycoside and amoxicillin, among others.¹⁸⁻²³ Amoxicillin is a beta-lactam antibiotic²⁴ and, like other penicillins, binds to and inhibits the carboxypeptidase and transpeptidase enzymes that are required for peptidoglycan biosynthesis (Figure S1).²⁵ The nitrogen-containing beta-lactam ring is designed to target the penicillin-binding membrane proteins (PBPs), which are involved in the cross-linking of the bacterial cell wall. Interestingly, amoxicillin is capable of reducing²⁶ Au(III) to Au(0) and stabilizing the resulting AuNPs due to high affinity of the amino groups to the gold surface.

Here we present the one-pot synthesis of amoxicillin-coated AuNPs (amoxi@AuNPs) that combined show enhanced photo-antimicrobial effect; i.e., highly reduced amount of antibiotic (typically 500 mg per dose are used), short irradiation time (~ 30 min) and high selectivity toward prokaryotic cells. Facile to prepare amoxicillin-coated AuNP were stable inside the bloodstream and tissue distribution, showing rapid clearance

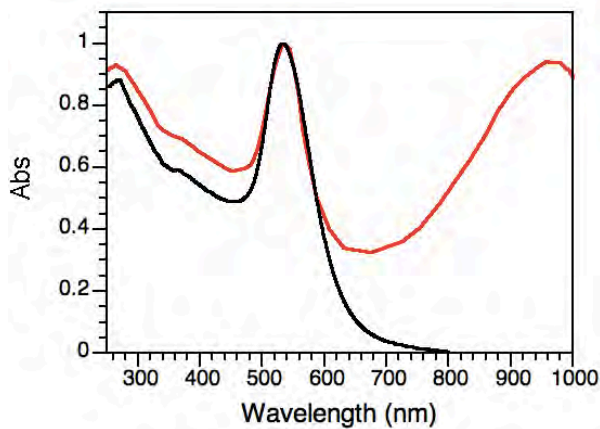
1 from the organism at the same time. In this sense, they are a better option
2 for clinical use in comparison to other stabilizing agents, such as glutathi-
3 one.²⁷ Furthermore, we introduce a novel method to check the selectivity of
4 the toxicity in a co-culture of bacteria and blood cells through time-resolved
5 fluorescence microscopy.

6 RESULTS AND DISCUSSION

7 Synthesis and characterization of amoxi@AuNPs

8 AuNPs were synthesized by thermal reduction utilizing amoxicillin
9 as both reducing and stabilizing agent. The absorption spectrum
10 (Figure 1) of the amoxi@AuNPs shows the characteristic plasmon
11 band of small spherical nanoparticles centered around 540 nm,
12 while the presence of a second absorption band around 950 nm can
13 account for the plasmon absorption bands of more complex
14 nanostructures, namely triangular, hexagonal and irregular polygo-
15 nal plates, including nanorods (see Figure S2-S4).²⁸

16 DLS measurements determined a hydrodynamic radius for the
17 amoxi@AuNPs of 79 ± 43 nm. The broad distribution of particle
18 sizes found by this technique is in agreement with the presence of
19 larger non-spherical nanostructures; in contrast to the AuNPs
20 synthesized with NaBH_4 ('unprotected' AuNPs) that show a more
21 monodisperse size distribution: 8 ± 2 nm. The positive Zeta poten-
22 tial value found for amoxi@AuNPs ($+30 \pm 7$ mV) confirms the
23 effectiveness of the amoxicillin as colloidal stabilizer.



24
25 Figure 1. Normalized absorption spectra of unprotected AuNP (black) and
26 of amoxi@AuNPs (red). The absorption wavelength at around 950 nm
27 accounts for the presence of non-spherical nanostructures.

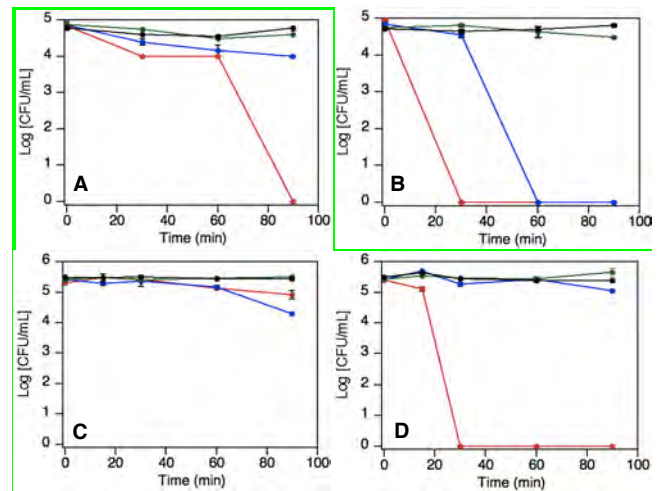
28 The conjugation of the stabilizer agent to the nanoparticle was
29 confirmed by FT-IR (see Figure S5). AuNPs showed ~11% amoxi-
30 cillin loading as determined by TGA. This amount is enough to
31 stabilize the particle but it is very low compared to the daily dose
32 administered to a patient (1-2 g) which could minimize all the
33 amoxicillin side effects.²⁹⁻³⁰

34 These new amoxi@AuNPs composites showed great stability in
35 different media such as PBS 37.5, 25%, 12.5% y 7.5% for 72 h, and
36 CMH 25% for 48 h, as well as CMH 12.5% and 7.5%; CTS 25%,
37 12.5% and 7.5% for 168 h and Milli-Q water, for 96 h. (Figure S6).
38 Nevertheless, they crashed immediately in all concentrated biologi-
39 cal media and PBS (100 and 50 %). Based on these findings, mi-
40 crobiological assays were carried out in 37.5 % PBS, which allows
41 the bacteria to be metabolically active and does not interfere with
42 the monitoring of the plasmon absorption.

43 In vitro studies

44 Antibacterial Activity

45 *Staphylococcus aureus* ATCC 29213 (MSSA) and a methicillin-
46 resistant clinical isolate of *Staphylococcus aureus* (MRSA) were
47 killed by 1.5 $\mu\text{g}/\text{mL}$ amoxi@AuNPs after only 30 min of irradiation
48 (Figure 2) with white light using an LED expo-panel (Figure S7).
49 This is considerably faster than other nano-photosensitizers we
50 have previously tested under similar exposure conditions.^{7, 10} It is
51 worth noting that light itself does not produce any damage or
52 change of the bacterial normal growth. The selection of white light
53 irradiation was based on the broad absorption spectrum shown by
54 the amoxi@AuNPs composites (Figure 1), ensuring the excitation
55 of most of the nanostructures present in the solution. Interestingly,
56 excitation using only green light (525 nm) did not produce antibac-
57 terial effect, thus the bactericidal effect requires the excitation of
58 more complex nanostructures using the full visible spectrum. Addi-
59 tionally, amoxi@AuNPs were able to kill all the MSSA after 90
60 minutes in the dark but not the MRSA. This could be a conse-
61 quence of the synergistic effect^{18, 31} between the antibiotic and the
62 nanoparticle, as amoxicillin alone was not bactericidal at this low
63 dose. It is important to highlight that the system temperature was
64 kept at 37-38°C during all the experimental procedures. Despite the
65 constant bulk temperature, it is well known that the excitation of
66 the surface plasmon of AuNPs can induce a localized heat on the
67 particle surface. Thus, the high local temperature experienced by
68 the bacteria in close proximity to the surface of the particle could
69 trigger their death.³² In fact, gold nanoparticles are able to convert
70 the absorbed light into heat very efficiently. These results in a hot
71 lattice and the temperature could increase up to tens of degrees,
72 enough to denaturalize biomolecules.³³⁻³⁵

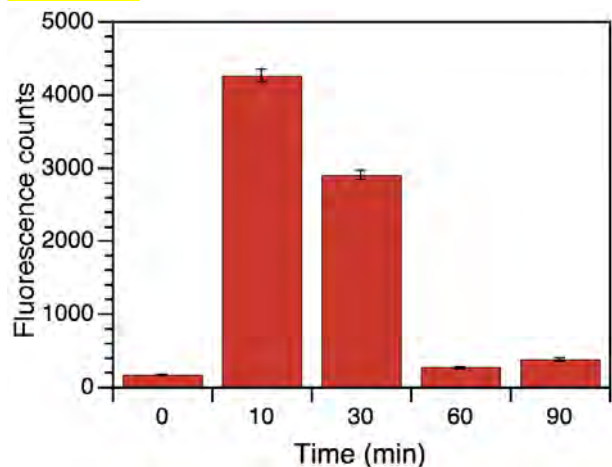


73
74 Figure 2. Bacterial growth over time of MSSA (A-B) and MRSA (C-D)
75 samples treated under dark conditions (A-C) and under LED illumination
76 (B-D) in the presence of 1.5 $\mu\text{g}/\text{mL}$ of amoxi@AuNPs (red), 0.15 $\mu\text{g}/\text{mL}$
77 amoxi@AuNPs (blue), and as control samples in the presence of amoxi-
78 cillin at the MIC (green) or PBS (black).

79 ROS quantification in bacterial culture

80 The generation of ROS was determined for samples of MRSA
81 phototreated with amoxi@AuNP (at bactericidal concentrations).
82 Figure 3 shows the maximum ROS production (almost 25 times
83 basal level) quantified after just 10 min of irradiation. This level of
84 ROS generation is even higher than the one observed for *S. aureus*
85 treated with AuNP and light.¹⁰ A significant amount of ROS for-
86 mation (almost 17 times basal level) can be formed after 30 min of
87 irradiation, although no bacterial growth was observed at that time.
88 This could be due to the presence of some bacteria organelles and

1 structures which global integrity and functionality are too damage
 2 to keep bacteria alive. After 60 min, ROS production is negligible.
 3 Dark levels are almost null (not shown). The temperature of all the
 4 samples (including the irradiated ones) was kept at 37°C during the
 5 whole experiment, avoiding the influence of macroscopic thermal
 6 effect. This significant amount of ROS detected could indicate that
 7 the bactericidal effect is in direct relation with the oxidative stress
 8 generated in bacteria when amoxi@AuNP (attached to their wall)
 9 are irradiated.



10

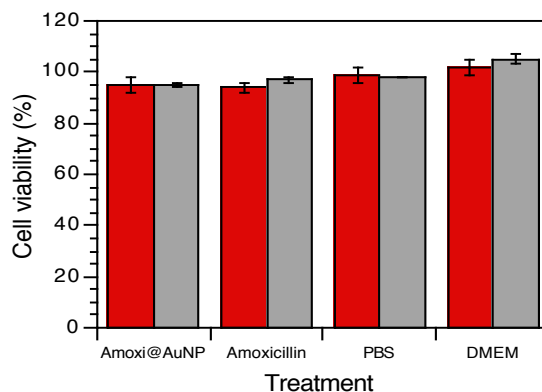
11 Figure 3. ROS production for samples of MRSA phototreated with
 12 amoxi@AuNP (at bactericidal concentrations).

13 Mammalian cell viability

14 The 3T3 cell line has become the standard fibroblast cell line since
 15 Todaro and Green originally obtained them from Swiss albino
 16 mouse embryo tissue in 1962.^{36 32} This line correspond to immor-
 17 talize cells; however, fibroblasts are much more sensitive to external
 18 factors than HeLa cells, most frequently used for *in vitro* experi-
 19 ments. For this reason, the activity of its mitochondrial enzymes, as
 20 evaluated by MTT assay, is an important parameter for the analysis
 21 of the effects of new drugs on eukaryotic cells as it is a reflection of
 22 potential toxicity to mammals. Figure 4 shows the effect of free
 23 amoxicillin, bare AuNPs and amoxi@AuNPs at their antibacterial
 24 or photo-antibacterial concentrations. Our results suggest that the
 25 cell viability of the samples with antibiotic or nanoparticles is simi-
 26 lar to control without drug (37.5 % PBS) and they all presented
 27 slightly less survival than the control with DMEM. Free amoxicillin
 28 was found to be non-toxic to other mammal cells in previous litera-
 29 ture reports while our own studies described the biocompatibility
 30 of uncoated AuNPs.^{10, 37}

31

32



33

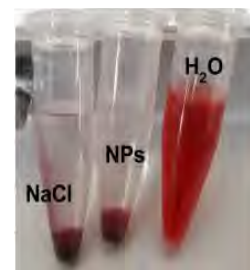
34 Figure 4. Cell survival (%) of fibroblast 3T3 treated with: 1.5 µg/mL
 35 amoxi@AuNP, 32 µg/mL amoxicillin, 37.5% PBS and DMEM, under 24 h
 36 of visible light irradiation (red) or under dark conditions (grey) for 24 h at
 37 37 °C, 5 % CO₂ and 95 % humidity.

38 Figure 4 shows that amoxi@AuNPs were not cytotoxic even under
 39 the same irradiation conditions used for the antimicrobial test.
 40 Similar results were found for gold nanoparticles embed in am-
 41 phiphilic block copolymers.³⁸ AuNPs are essentially harmless when
 42 compared to other antimicrobial nanoparticles, such as zinc nano-
 43 particles, which have a substantial toxic impact to human fibroblast
 44 after 24 h.³⁹ This demonstrates that the proposed photosensitizer is
 45 selectively toxic for bacteria and does not affect eukaryotic cells to
 46 any significant extent, due to the absence of any penicillin-binding
 47 protein 1A on the eukaryotic membrane.

48 Parenteral and intraperitoneal injection of nanoparticles can pro-
 49 duce high local concentration and broad distribution in the circu-
 50 lating blood, leading to the need for evaluation of their biological
 51 safety. Ex vivo experiments on whole blood were conducted be-
 52 cause erythrocytes together with other blood cells and serum con-
 53 tent reflect properly the actual conditions in mammals organism.⁴⁰
 54 Experiments were performed at t = 0, 2, 5 and 24 h in the dark and
 55 under LED irradiation, with the bactericidal concentration of
 56 amoxi@AuNP (1.5 µg/mL). Total hemolysis was established by
 57 adding H₂O to the red blood cell (RBC) samples; n=3; SD<0.1.
 58 See Figure S7 for illumination details. The tested amoxi@AuNPs
 59 did not produce any alteration to the red blood cells, as shown in
 60 Table 1. There was no hemolysis at all, even under irradiation
 61 conditions. Thus, the amoxi@AuNPs are selectively toxic for bacte-
 62 ria and do not affect erythrocytes. Under these illumination condi-
 63 tions, the photo-thermal effect is then harmless for eukaryotic cells.

64 Table 1. Hemolysis percentage (%) of blood samples treated
 65 with 1.5 µg/mL amoxi@AuNP and with 0.9 % NaCl as negative
 66 control and H₂O as positive control

T	Control	Amoxi@AuNPs	Control	Amoxi@AuNPs
0 h	1.3	1.2	1.2	1.3
2 h	1.3	1.3	1.3	1.4
5 h	1.2	1.2	1.2	1.2
24 h	1.3	1.2	1.2	0.9
LED	OFF	ON	OFF	ON



67

1 In order to further prove that amoxi@AuNPs are selectively toxic 30
 2 for bacteria, co-cultures with blood cells were treated with the 31
 3 particles under the same irradiation conditions. The FLIM techni- 32
 4 que is extremely useful in bioimaging, where, for instance, light 33
 5 scattering can interfere with steady-state fluorescence imaging. The 34
 6 fluorescence lifetime can change depending on the fluorophore 35
 7 environment and hence the same fluorophore can be tracked in 36
 8 different locations utilizing the same emission wavelength. Here we 37
 9 use this technique together with a well-known DNA and RNA 38
 10 intercalator, acridine orange (AO-see Figure S8).⁴¹ Concentrations 39
 11 of AO around 0.3 mg/mL (1 mM) or higher lead to the formation 40
 12 of non-fluorescent dimers.⁴² However, AO can intercalate in nucle- 41
 13 ic acid helices as the cationic monomer can presumably bind 42
 14 through electrostatic interaction with negatively charged phos- 43
 15 phate. This interaction recovers the AO fluorescent properties and 44
 16 is the reason why AO is extensively used as a biological stain in 45
 17 fluorescence microscopy. When bound to ssDNA, AO shows a 46
 18 stable emission maximum at 630 nm upon excitation at around 458 47
 19 nm. Interestingly, AO, when externally bound to disorganized or 48
 20 broken genetic material is energetically less stable and is also very 49
 21 weakly emissive.⁴³ Here, AO was found to bind to the genetic mate- 50
 22 rial in both live bacteria and cells showing emission around 630 nm 51
 23 upon excitation at 440 nm. When the cells are subjected to damage, 52
 24 the genetic material of a dead cell is severely disrupted if not com- 53
 25 pletely disintegrated. As a consequence, the AO most likely spreads 54
 26 into the solution as the non-fluorescent dimer forms or remains 55
 27 externally bound to the remaining DNA/RNA bases producing a 56
 28 weak and short emission. Interestingly, the lifetime of the emissive 57
 29 structures is different when the AO is attached to live bacteria (~3-

7 ns), live white blood cells (~7-14 ns), or bound externally to the 30
 31 disrupted genetic material of dying cells (<3 ns) with a lifetime 32
 33 almost as short as free AO.⁴⁴ Thus, using time-resolved fluores- 34
 35 cence techniques we were able to differentiate live bacteria or 36
 37 eukaryotic cells from dead ones. 38

39 According to the lifetime color scale at the bottom of Figure 5, 40
 41 groups of *S. aureus* appeared bright green while alive (Figure 5-A) 42
 43 and the few dead *coccus* that are dead but were not completely 44
 45 broken by photothermal effect of PACT appeared blue (Figure 5- 46
 47 B), indicating a decrease in the AO emission lifetime. Live erythro- 48
 49 cytes (without nucleus or genetic material) were observed as pale 50
 51 green rings (Figure 5-C, D and E) and were not found heating in 52
 53 the control sample (Figure 5-F). The same sample presented a 98 54
 55 % of hemolysis in parallel measurements. Lymphocytes were ob- 56
 57 served as bright yellow-orange spots when alive (Figure 5-C, D and 58
 59 E) and pale green spots when dying or damaged (Figure 5-F). A 60
 61 larger white blood cell (eosinophil) was observed alive (Figure 5- 62
 63 E). Its nucleus appeared dull green because of the lax chromatin 64
 65 content; however, the AO presented longer lifetimes, up to 14 ns in 66
 67 the cytoplasm due its strong interaction with eosinophilic granules, 68
 69 described by Ueki et al⁴⁵ and previously by Robbins et al.⁴⁶ The 70
 71 aforementioned difference in the emission lifetime of AO was 72
 73 developed as a practical and fast method to study the survival of 74
 75 both eukaryotic and prokaryotic cells together. It requires just one 76
 77 fluorescent dye, one excitation laser and one emission filter, in 78
 79 contrast to other similar techniques that excite AO with different 80
 81 lasers and need other fluorescent dyes as ethidium bromide or 82
 83 propidium iodide as contrast agents.⁴⁷⁻⁴⁸

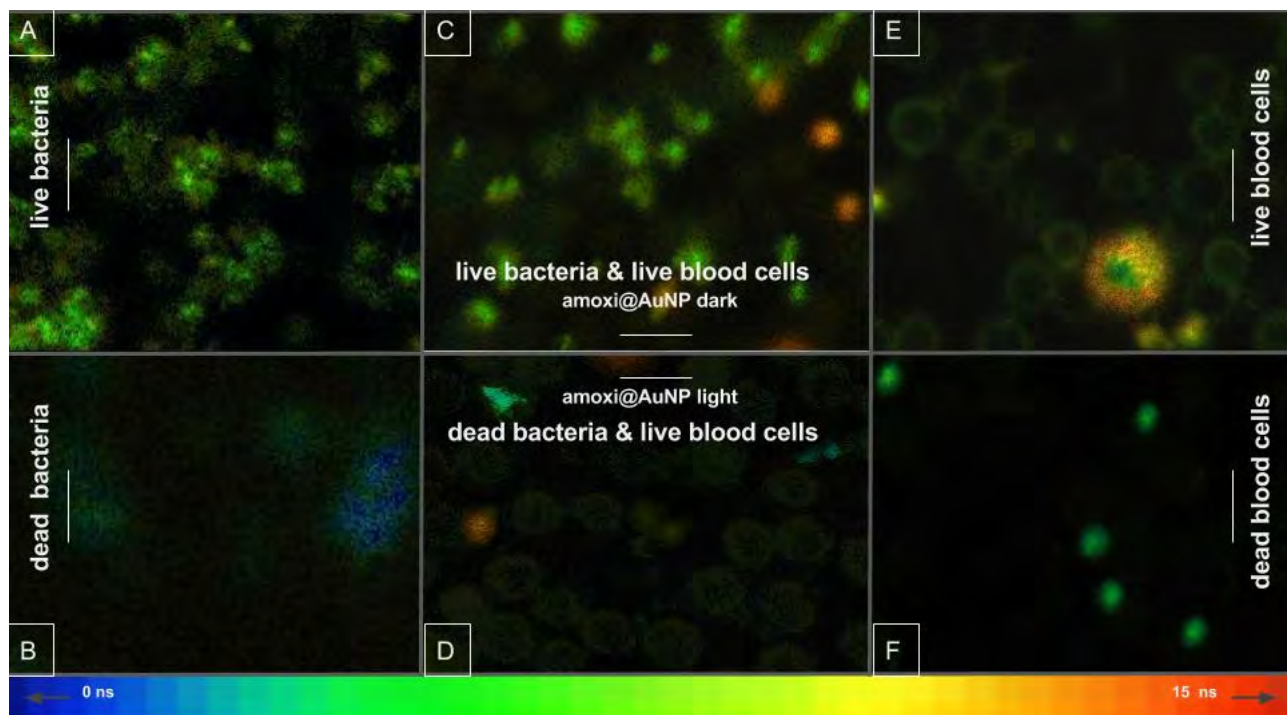


Figure 5. FLIM images of biological samples containing AO: co-culture of *MSSA* and blood cells treated with amoxi@AuNP for 30 min in darkness conditions (C) and under irradiation (D), *S. aureus* suspension treated with amoxi@AuNP for 30 min in darkness conditions (A) and under irradiation (B), blood cells treated with amoxi@AuNP for 30 min in darkness conditions (E) and heated at 80 °C (F). Color gradient bar at the bottom indicates lifetime of AO emission in ns. Scale bar: 20 μ m.

In vivo studies

The distribution of the nanoparticles in internal organs is crucial to determine their *in vivo* stability and fate after the desired activity is

completed. Following IP injection (see experimental section), amoxi@AuNPs were found using TEM analysis (Figure 6) inside the liver (rows A and B), the kidney (rows C and D) and the spleen (rows E and F). Importantly, they did not go through the brain blood barrier as amoxi@AuNPs were not found in brain tissue (data not shown). In general, the nanoparticles were internalized in vesicles in Kupffer cells in the liver just 2 h after IP injection. Usually, hepatobiliary system represents the main route of excretion for particles that do not undergo renal clearance.⁴⁹ Nanoparticles of diameter equal or less than 100 nm, smaller than the pore size of liver fenestrae, could have easily penetrated through the endothelial wall too. At the same time, some amoxi@AuNPs were found in the spleen, indicating that they had been carried there earlier by the phagocytic cells. However, for these nanoparticles our results indicate that the largest NPs amount was found in the kidneys (2 h post injection) being internalized in vesicles after having gone through the microvilli. Only a small fraction of the nanoparticles was found in the samples taken 5 h after administration. This could be due to the elimination in urine (vide infra) or as result of normal process

of vesicle degradation, since shrunken vesicles were observed (Figure 6-IIIC/IIID). In kidneys and the spleen, where a few nanoparticles were interacting with the dense chromatin, around 5 % of pyknotic nuclei were observed (n=1008 cells), possibly as a consequence of the oxidative-stress generated by the nanomaterial.⁵⁰ It is noteworthy that after 24 h, all three organs presented normal histopathology. Their different composing cells (including hepatocytes, epithelial and endothelial cells, podocytes, macrophages and red and white blood cells) looked unaltered and were of normal size and structure. The AuNP without antibiotic stabilization were only found in small quantities in the liver at 2 h, indicating their poor stability in biological fluids after injection. According to our results, coating of AuNP is necessary to improve their *in vivo* stability. To obtain a global characterization, 2 grids were prepared per each organ (2 organs per each condition) and over 300 TEM pictures were taken. The more representative ones were selected to illustrate the path of the nanoparticles through the tissues studied (Figure 6).

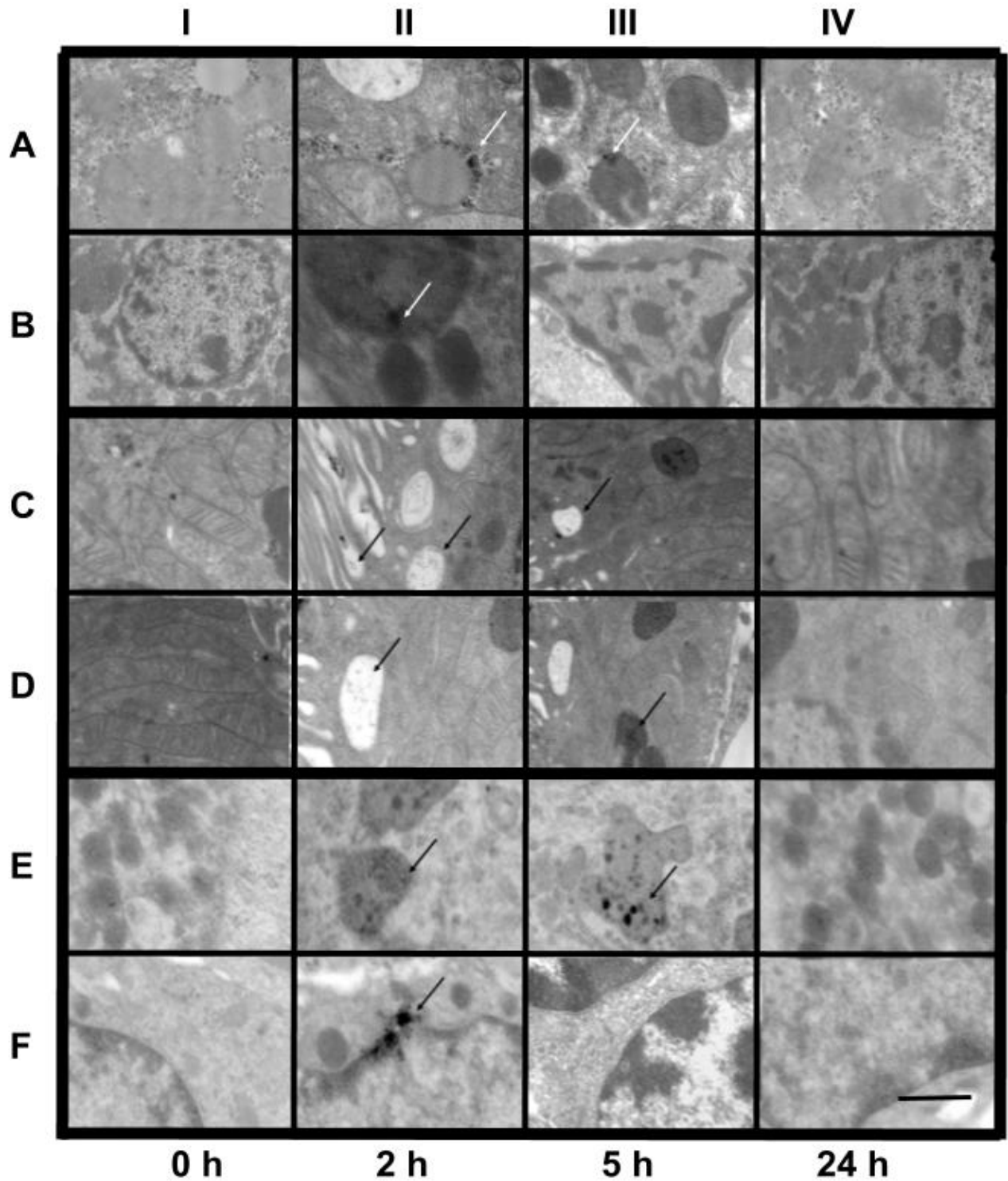


Figure 6. Representative TEM pictures of rat tissue samples showing the biodistribution of amoxi@AuNPs in the liver (rows A and B), kidneys (rows C and D) and spleen (rows E and F) after intraperitoneal injection. Scale bar is the same (1 μm) for all pictures.

1 Additionally, particles larger than the effective pore size in normal
2 intact endothelium (5 nm), such as those used here, experience
3 prolonged circulatory times due to slow transportation across the
4 endothelium; therefore, the study of their effect on blood cells is
5 quite relevant. Cell counting (Table 2) on samples of rats injected
6 with nanoparticles (Group I and Group II) was not different from
7 the control animals (Group III), except for a slight increase in the
8 number of neutrophils (10 % over top reference value, $p < 0.05$) in
9 Group II at 2 h. This is correlated with the observation of active
10 phagocytic cells in the liver, kidneys and spleen at the same time.
11 The elevation in neutrophils may be due to the host response to the
12 injection and distribution of amoxi@AuNPs. Normal values were
13 totally restored after 24 h, as a sign of complete elimination of the
14 nanoparticles from the organism. According to microscope obser-

1 vation of smears, red blood cells from Group I and II kept their
2 integrity, suggesting that they were not stressed by the nanomateri-
3 al. This finding is in agreement with the ex vivo hemolysis test
4 results.

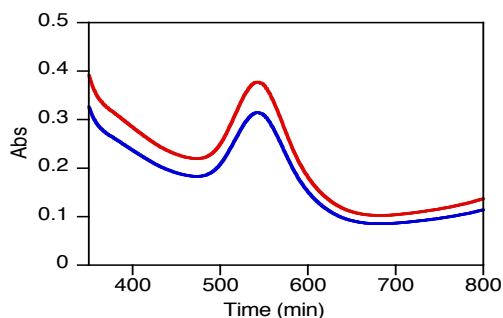
5 **Table 2. Cell counting (%) from blood smears of rats treated**
6 **with AuNP (I), amoxi@AuNP (II) and physiological saline**
7 **solution (III).**

%	Ref*	2 h			5 h			24 h		
		I	II	III	I	II	III	I	II	III
N	1--16	18	26	5	12	16	6	10	11	6
L	82-96	82	74	94	86	82	93	89	87	92
M	0-3	0	0	1	2	2	0	0	2	2
E	0-2	0	0	0	0	0	1	1	0	0
B	0	0	0	0	0	0	0	0	0	0
S.N	0-1	0	0	0	0	0	0	0	0	0

8 * "Ref" are the reference values for healthy male Wistar rats.

9 N (neutrophils), L (lymphocytes), M (monocytes), E (eosino-
10 phils), B (basophils), SN (segmented neutrophils).

11 Finally, renal excretion is the desirable pathway for AuNP removal,
12 because it would keep the catabolism or breakdown to a minimum,
13 avoiding possible side effects.⁴⁹ Renal clearance, as a fundamental
14 part of drug elimination is determined by the molecular chemical
15 and physical properties, including size, surface charge, and surface
16 chemistry.⁵¹ Without such clearance or their biodegradation into
17 biologically benign components, the toxicity potential increases. To
18 address this concern, qualitative detection of intact nanoparticles in
19 urine was done by measuring their plasmon absorption (Figure 7).
20 Urine samples from Group II showed an absorption peak (abs <
21 0.40) at 540 nm, consistent with spherical AuNP after 5 h of IP
22 injection. Apparently, other shapes and sizes would preferably be
23 up-taken by cells and degraded inside vesicles as shown in TEM
24 pictures. It seems that most of the nanomaterial is being eliminated
25 between 2-5 h after injection, because the plasmon peaks are not
26 bigger in urine samples collected after one day of injection than in
27 those collected after 5 h; in agreement with previous report⁵² Both
28 works suggest that the kidneys are the primary sites for clearance of
29 the smallest particles, followed by the hepatobiliary system. No
30 bare AuNP were found in urine collected from Group I, supporting
31 the hypothesis that uncoated AuNP are not being well distribut-
32 ed/eliminated. In summary, amoxicillin is not only helping to the
33 stabilization of the nanoparticles, but also to their renal clearance.



35 Figure 7. Absorption spectra of amoxi@AuNPs from rat urine collected
36 after 5 h (blue) and 24 h (red) of IP injection and resuspended in 37.5 %
37 PBS.

38 CONCLUSIONS

39 The combination of *in vivo* and *in vitro* studies presented here
40 showed that amoxi@AuNPs are suitable nanostructures for PACT
41 applications. amoxi@AuNPs can be easily synthesized in one pot
42 utilizing amoxicillin as both reducing and stabilizing agent. The
43 particles are stable in biological media and show photoinduced
44 antibacterial activity (irradiation time ~30 min), even against AR
45 strains. Importantly, amoxi@AuNPs are very biocompatible with
46 eukaryotic cells under PACT conditions. The bacterial death is
47 believed to occur upon localized surface plasmon excitation of the
48 AuNP. The antibiotic was used as a reducing agent for the synthesis
49 of AuNPs and its presence confers the NP with the selectivity
50 toward the bacterial cell. This is a major advantage when combat-
51 ting microorganism that produce lytic enzymes, developing antibi-
52 otic resistance. Accordingly, the amoxi@AuNPs can act faster than
53 silver and zinc nanoparticles tested by other groups without plas-
54 mon excitation,⁵³ showing their potential as antibacterial agents.

55 We have also demonstrated that FLIM can be very useful to deter-
56 mine the cell selectivity and bactericidal activity in prokaryot-
57 ic/eukaryotic co-cultures by a rapid and simple analysis. This analy-
58 sis only requires one fluorescent dye, one excitation laser and one
59 emission filter, in contrast to similar techniques that excite AO with
60 different lasers and need other fluorescent dyes as ethidium bro-
61 mide or propidium iodide as contrast agents.

62 Finally and yet importantly, our results show that the injected
63 AuNP have a faster clearance rate than other similar
64 nanomaterials⁵⁴⁻⁵⁵ and have not induced considerable cytotoxicity
65 responses. As a result, amoxi@AuNPs seem to have a low potential
66 of accumulation in mammal organisms. These findings are remark-
67 ably useful for the potential development of pharmaceutical formul-
68 ations.

69 EXPERIMENTAL SECTION

70 Materials

71 Tetrachloroauric acid-99% (HAuCl₄) was purchased from Sigma-
72 Aldrich, Trihydrate Amoxicillin from Todo Droga, (Argentina). Mueller
73 Hinton broth (MHB), Tryptic Soy broth (TSB), Tryptic Soy agar (TSA),
74 Brain Heart infusion (BHI), Luria Bertani broth (LBB) and Phosphate
75 Buffer Saline (PBS) were purchased from Britania (Argentina).

76 Synthesis of amoxi@AuNPs and AuNP

77 Antibiotic coated nanoparticles were prepared with amoxicillin in one-
78 step synthesis that uses the antibiotic as both the reducing and stabilizer
79 agent. This bottom-up method is based on the reduction of the gold pre-
80 cursor (HAuCl₄ 100 μL, 10 mM) with amoxicillin trihydrate (900 μL, 0.1
81 mM) at 50 °C for 18 minutes. This corresponds to a 16 wt% of amoxicillin
82 with respect of the mass of Au. All solutions were freshly prepared prior to
83 the synthesis and left to stabilize at room temperature for 30 minutes
84 before heating. Three cycles of Milli-Q water washing and centrifugation
85 were used to remove unbound amoxicillin molecules. unprotected

86 In order to obtain 500 mL of 0.2 mM bare AuNP, 1 mL of 0.1 M
87 HAuCl₄ aqueous solution was added to 500 mL of previously cooled Milli-
88 Q water (8 °C). Then, 10 mL of a NaBH₄ (0.13 M) solution was trans-
89 ferred dropwise to the flask.

90 Characterization of amoxi@AuNP

91 The changes of the surface plasmon resonance of the resuspended pellet
92 and the absorption spectrum of the amoxicillin molecules present in the
93 supernatant were monitored using a Cary 60 UV-Vis spectrophotometer.
94 Shape and size of the synthesized AuNP were performed through Trans-
95 mission Electron Microscopy (TEM-Jeol 1200 EX II). Samples for TEM
96 measurements were prepared by placing a 4 μL drop of the amoxi@AuNP
97 solution on carbon-coated copper grids and left to dry completely at 37 °C
98 in a drying oven. At least 400 nanoparticles were analysed statistically using
99 ImageJ software. On the same samples, zeta potential and dynamic light
100 scattering (DLS) were measured with a Malvern Zetasizer (model Nano-

S). The binding of amoxicillin to AuNP was analyzed by Fourier Transform Infrared (FT-IR) spectroscopy in transmission mode using a Nicolet iN 10 spectrophotometer. Samples of amoxicillin trihydrate, bare AuNP and amoxi@AuNPs were freeze-dried and then measured by FT-IR at low temperature.

The amount of amoxicillin was determined by Thermogravimetric Analysis (TGA). For this, 4 mL of 1.5 µg/mL of the amoxi@AuNPs were centrifuged down and pellets were combined to be exhaustively dried in a desiccator for 48 h prior to TGA at 10 °C/min from 25 to 1000 °C under nitrogen atmosphere (flow rate of 25 mL/min) with a TA-THA Q5000.

Colloidal stability

Stability measurements of amoxi@AuNPs (1.5 µg/mL) in different buffer solutions and growth media were conducted based on the change in plasmon absorbance maxima at different time points, utilizing UV-Vis spectrophotometry. Stability was considered as the time it took for a 20% decrease in plasmon absorption at the wavelength on the initial maximum absorbance.⁸ The stability measurements were carried out (using a Biotek plate reader) for 7 days (time = 0, 0.5, 1, 2, 4, 6, 12, 18, 24, 48, 72, 120, 144, 168 h) in Milli-Q water, saline solution, PBS buffer solution (pH=7), Mueller Hinton Broth (MHB) and Tryptic Soy Broth (TSB) at different concentrations (100, 50, 25, 12.5 %). In order to avoid contamination, the stability measurement of nanoparticles dispersed in growth media were conducted under sterile conditions.

Bacterial strains and growth conditions

The experiments were performed using *Staphylococcus aureus* ATCC 29213 (MSSA ATCC 29213) and a methicillin-resistant clinical isolate of *Staphylococcus aureus* (MRSA 9455). Clinical isolate was supplied by the Bacteriology Service of Sanatorio Aconcagua, Córdoba, Argentina. Stock cultures were maintained in TSB and stored in a freezer in 10% glycerol.

Antibacterial Capacity

Antibacterial activity of novel amoxi@AuNPs against MSSA and MRSA was tested. Bacterial suspensions of 10⁸ colony forming units per mL (CFU/mL) in 37.5% PBS (pH=7) from a single colony of each strain were prepared. Using a 96 well plate, 100 µL of bacterial suspension and 100 µL of the tested solutions (37.5% PBS, 0.15 µg/mL, amoxi@AuNPs, 1.5 µg/mL amoxi@AuNPs and amoxicillin at minimum inhibitory concentration (MIC) per each strain as control: 2 µg/mL for MSSA and 32 µg/mL for MRSA) were mixed and irradiated for a total of 90 min under white LED illumination at 37 °C. Control experiments were run under the same conditions in the dark. All samples were run in triplicates. Aliquots of each sample were diluted properly and seeded in TSA plates. CFU were counted from the agar after 24 h of incubation at 37 °C.

incubation at 37 °C.

ROS quantification in bacterial culture

The pre-fluorescent probe dihydrorhodamine 123 (DHR) was chosen for its high sensitivity to quantify total ROS and Reactive nitrogen species (RNS).⁵⁶ This dye diffuses passively through most of cell membranes, where DHR generates a fluorescent green signal at 536 nm when oxidized. Radical indicators of oxidative stress were measured with DHR (1 µM) in bacterial suspensions (10⁹ CFU/ml) treated with a 1.5 µg/mL of amoxi@AuNPs. Samples were irradiated for 10, 30, 60 and 90 min.

Cell Viability

The 3T3 fibroblasts were cultured in Dulbecco Modified Essential Medium (DMEM) with 10 % calf serum. Cells were grown until 85% to 95% confluence, then washed with phosphate-buffer saline (Invitrogen) and trypsinized with 1 mL of 0.05% trypsin, 0.53 mM ethylenediaminetetraacetic acid, phenol red. Trypsinization was stopped by adding fresh medium to the reaction. The cells were washed twice by centrifugation with DMEM without serum, resuspended in medium without serum and plated at approximately 10⁵ cells/per well after proper cell counting in an Improved Neubauer chamber. They were incubated overnight to allow attachment and then treated with 1.5 µg/mL amoxi@AuNP, 32 µg/mL amoxicillin, 37.5% PBS and DMEM and irradiated with a white LED for 24 h. Cells were kept in the dark for 24 h at 37 °C, 5 % CO₂ and 95 % humidity. MTT assay based on the reduction of tetrazolium salt to formazan crystals in living cells was done according to a Sigma protocol to determine the

percent survival.⁵⁷ The absorbance spectra on the different wells were measured using a Biotek plate reader.

Hemolysis

The integrity of red blood cells from human healthy volunteers (from Córdoba, Argentina) incubated with amoxi@AuNPs 1.5 µg/mL with and without irradiation, was evaluated following a procedure previously described⁵⁸ with slight modifications. The amoxi@AuNPs had to be removed by centrifuging the samples before reading the absorbance of the free hemoglobin (541 nm) to avoid spectral interference. Measurements were made at 0, 2, 5 and 24 h by triplicates. An aqueous solution of 0.9% NaCl and H₂O were used as negative and positive control of hemolysis, respectively.

Fluorescence Lifetime Imaging Microscopy (FLIM) study on co-cultures of blood cells and bacteria

Acridine orange (AO) was employed due to its characteristic fluorescence emission when intercalated in DNA or RNA.⁵⁹⁻⁶⁰ FLIM imaging of the dye was introduced as a method to check the viability of blood cells (anticoagulated fresh samples from healthy volunteers from University of Córdoba) and bacteria (10⁷ CFU/mL of *S. aureus* 29213) cultured together and treated with irradiated and non-irradiated amoxi@AuNPs (1.5 µg/mL). The samples were studied using a Fluorescent Lifetime Imaging System (FLIM, PicoQuant Microtime 200). The instrument is equipped with a frequency doubled picosecond pulse diode laser (440 ± 10) nm, 70 ps, 40 MHz, LDH-D-C-440, PicoQuant). The laser beam was collimated and focused through a fiber-coupling unit. A beam splitter Z440 bcm (Chroma) was used to reflect the excitation light into the oil immersion TIR (total internal reflection) objective (100x, NA1.45, Olympus, PLAPO). The excitation dose (average power) is about 0.6 mW for all samples. Emission was collected between 610-680 nm using the ET645/75BP emission filter. Briefly, 100 µL of the biological sample and 100 µL of AO (1 mg/mL) were mixed and incubated at room temperature for 5 minutes. Lifetimes longer than 5 ns were found for live bacteria and cells, while dead bacteria or cells can be detected by a decrease in the emission intensity and lifetime of unbound AO produced by disorganization of the spread genetic material in necrotic or broken cells. Aliquots of the dye alone or mixed with amoxi@AuNPs were also tested for fluorescence. Fresh samples of blood cells or PBS suspension of bacteria in the absence of nanoparticles were run as controls for "alive samples". Accordingly, the same samples were also heated up to 80 °C and imaged as "dead samples control". Furthermore, bacterial growth in the observed samples was also ruled out by CFU counting in MH agar plates while integrity of eukaryotic cells was monitored by parallel hemolysis measures.

Biodistribution of nanoparticles

Male Wistar rats with a body weight of 280-310 g at the time of drug administration, were maintained in the animal house facility at the *Departamento Farmacología*, Córdoba, Argentina (Food and water provided ad libitum at a constant temperature 22 ± 2 °C with 12 h by 12 h light and dark cycle). The rats were handled for one week for acclimatization. At the beginning, the rats were divided into 3 groups of 2 rats each: Group I was subjected to intra-peritoneal injection with 34 µg/mL AuNP, Group II with 1.5 µg/mL amoxi@AuNPs and Group III with physiological saline solution as control. After 2, 5, and 24 h post-injection, two animals from each group were anaesthetized using a mix of 55 mg/kg ketamine and 11 mg/kg xylazine. Immediately, cardiac perfusion with PBS (0.1 M) was carried out to remove all red blood cells from their internal organs. Finally, after proper fixation (35 minutes of perfusion with 2 % paraformaldehyde and 2 % glutaraldehyde in PBS) the liver, heart, kidney, spleen, and brain were harvested. TEM pictures were taken with a TEM-Zeiss-906E microscope. All experiments on animals were conducted complying the ARRIVE guidelines and were carried out in accordance with the National Institutes of Health guide for the care and use of Laboratory animals (NIH Publications No. 8023, revised 1978) and the Guide for the Care and Use of Laboratory Animals (Eighth Edition, 2011).⁶¹

Biocompatibility with blood cells

Previous to perfusion, blood smears (triplicates) were made from fresh blood extracted through a cardiac puncture.⁶² Samples were stained with May Grunwald/Giemsa and analyzed under an optical microscope. Results reported are the averages of quadruplicates. Student t-test was performed

1 to detect differences that were considered statistically significant when P
2 values were lower than $\alpha=0.05$.

3 Renal clearance

4 At the same time intervals (2, 5 and 24 h), urine was collected using
5 metabolic boxes. The plasmon absorption of the AuNP was measured by
6 spectroscopy using a multi-well spectrophotometer (Biotek), by centrifug-
7 ing the collected urine and resuspending the pellet in 0.5 mL of 37.5 % PBS.
8

9 AUTHOR INFORMATION

10 ORCID Numbers

11 **M. C. Becerra: 0000-0003-2853-4437**

12 M. J. Silvero C.: 0000-0003-1585-2989

13 A. E. Lanterna: 0000-0002-6743-0940

14 J. C. Scaiano: 0000-0002-4838-7123

15 Author Contributions

16 All authors have approved the final article. Conflict of interest: none.

17 Funding Sources

18 This work was supported in Argentina by grants from CONICET (PIP
19 2012–2014) grant no. 11220110100965, SECyT-UNC, and FONCyT
20 (PICT 2014) grant no. 821 to Dr. Becerra, SECyT-UNC to Dr. Perez
21 and in Canada thanks to the Natural Sciences and Engineering Re-
22 search Council of Canada through its Discovery programs and the
23 Canada Research Chairs program. MCB and MFP are career research
24 members of CONICET. MJSC is especially grateful to CONICET for
25 the postdoctoral fellowship and the scholarship awarded to visit the
26 University of Ottawa. DMR and EAV have doctoral fellowships from
27 SECyT-UNC.

28 ASSOCIATED CONTENT

29 Supporting information

30 The Supporting Information is available free of charge on the [ACS](#)
31 [Publications website](#) at DOI:

32 Details of the experimental procedures, IR spectra, TEM images and
33 size distribution graphs.
34

35 ACKNOWLEDGMENT

36 The authors are grateful to Estela Salde and Lorena Mercado for their
37 laboratory technical assistance with the *in vivo* experiments and to Dr.
38 Cristina Maldonado for her help in TEM samples preparation and
39 analysis.

40 REFERENCES

41 1. Lutgring, J. D.; Granados, C. A. D.; McGowan, J. E.,
42 Antimicrobial Resistance: An International Public Health Problem. In
43 *Antimicrobial Drug Resistance: Clinical and Epidemiological Aspects, Volume*
44 *2*, Mayers, D. L.; Sobel, J. D.; Ouellette, M.; Kaye, K. S.; Marchaim, D., Eds.
45 Springer International Publishing: Cham, 2017; pp 1519-1528.
46 2. Spellberg, B.; Guidos, R.; Gilbert, D.; Bradley, J.; Boucher, H.
47 W.; Scheld, W. M.; Bartlett, J. G.; Edwards, J. J., The Epidemic of
48 Antibiotic-Resistant Infections: A Call to Action for the Medical
49 Community from the Infectious Diseases Society of America. *Clin. Infect.*
50 *Dis.* **2008**, *46* (2), 155-164.
51 3. WHO *Antimicrobial resistance: global report on surveillance 2014*;
52 2014; p 257.
53 4. Suresh, A. K., *Metallic nanocrystallites and their interaction with*
54 *microbial systems*. Dordrecht: Springer: 2012; p 67.
55 5. Bucharskaya, A.; Maslyakova, G.; Terentyuk, G.; Yakunin, A.;
56 Avetisyan, Y.; Bibikova, O.; Tuchina, E.; Khlebtsov, B.; Khlebtsov, N;

Tuchin, V., Towards Effective Photothermal/Photodynamic Treatment
Using Plasmonic Gold Nanoparticles. *Int. J. Mol. Sci.* **2016**, *17* (8).

6. Huang, X. H.; El-Sayed, I. H.; Qian, W.; El-Sayed, M. A., Cancer
cell imaging and photothermal therapy in the near-infrared region by using
gold nanorods. *J. Am. Chem. Soc.* **2006**, *128* (6), 2115-2120.

7. Fasciani, C.; Silvero, M. J.; Anghel, M. A.; Arguello, G. A.;
Becerra, M. C.; Scaiano, J. C., Aspartame-Stabilized Gold-Silver Bimetallic
Biocompatible Nanostructures with Plasmonic Photothermal Properties,
Antibacterial Activity, and Long-Term Stability. *J. Am. Chem. Soc.* **2014**,
136 (50), 17394-17397.

8. Weerasekera, H. D.; Silvero, M. J.; da Silva, D. R. C.; Scaiano, J.
C., A database on the stability of silver and gold nanostructures for
applications in biology and biomolecular sciences. *Biomater. Sci.* **2017**, *5*
(1), 89-97.

9. Silvero, M. J.; Argüello, G. A.; Becerra, M. C., Photodynamic
Antibacterial Chemotherapy (PACT) Using Gold Nanoparticles and LED's
Irradiation. *J. Nanopharm. Drug Deliv.* **2014**, *2* (2), 148-152.

10. Silvero, M. J.; Becerra, M. C., Plasmon-induced oxidative stress
and macromolecular damage in pathogenic bacteria. *RSC Adv.* **2016**, *6*
(102), 100203-100208.

11. Shi, X. L.; Zhu, Y. T.; Hua, W. D.; Ji, Y. L.; Ha, Q.; Han, X. X.;
Liu, Y.; Gao, J. W.; Zhang, Q.; Liu, S. D.; Ren, K. L.; Wu, X. C.; Li, H. Y.;
Han, D., An *in vivo* study of the biodistribution of gold nanoparticles after
interstitial space injection in the tarsal tunnel. *Nano Res.* **2016**, *9* (7),
2097-2109.

12. Khlebtsov, N.; Dykman, L., Biodistribution and toxicity of
engineered gold nanoparticles: a review of *in vitro* and *in vivo* studies.
Chem. Soc. Rev. **2011**, *40* (3), 1647-1671.

13. Aydın, A.; Sipahi, H.; Charehsaz, M., Nanoparticles Toxicity
and Their Routes of Exposures. In *Recent Advances in Novel Drug Carrier*
Systems, Sezer, A. D., Ed. InTech: Rijeka, 2012; p Ch. 18.

14. Opanasopit, P.; Nishikawa, M.; Hashida, M., Factors affecting
drug and gene delivery: Effects of interaction with blood components. *Crit.*
Rev. Ther. Drug Carrier Syst. **2002**, *19* (3), 191-233.

15. De Jong, W. H.; Hagens, W. L.; Krystek, P.; Burger, M. C.; Sips,
A. J. A. M.; Geertsma, R. E., Particle size-dependent organ distribution of
gold nanoparticles after intravenous administration. *Biomaterials* **2008**, *29*
(12), 1912-1919.

16. Wang, L. M.; Li, Y. F.; Zhou, L. J.; Liu, Y.; Meng, L.; Zhang, K.;
Wu, X. C.; Zhang, L. L.; Li, B.; Chen, C. Y., Characterization of gold
nanorods *in vivo* by integrated analytical techniques: their uptake,
retention, and chemical forms. *Anal. Bioanal. Chem.* **2010**, *396* (3), 1105-
1114.

17. Sharifi, S.; Behzadi, S.; Laurent, S.; Forrest, M. L.; Stroeve, P.;
Mahmoudi, M., Toxicity of nanomaterials. *Chem. Soc. Rev.* **2012**, *41* (6),
2323-2343.

18. Gu, H. W.; Ho, P. L.; Tong, E.; Wang, L.; Xu, B., Presenting
vancomycin on nanoparticles to enhance antimicrobial activities. *Nano*
Lett. **2003**, *3* (9), 1261-1263.

19. Kalita, S.; Kandimalla, R.; Sharma, K. K.; Katakai, A. C.; Deka,
M.; Kotoky, J., Amoxicillin functionalized gold nanoparticles reverts MRSA
resistance. *Mater. Sci. Eng. C Mater. Biol. Appl.* **2016**, *61*, 720-727.

20. Grace, A. N.; Pandian, K., Antibacterial efficacy of
aminoglycosidic antibiotics protected gold nanoparticles - A brief study.
Colloids Surf, A **2007**, *297* (1-3), 63-70.

21. Brown, A. N.; Smith, K.; Samuels, T. A.; Lu, J.; Obare, S. O.;
Scott, M. E., Nanoparticles Functionalized with Ampicillin Destroy
Multiple-Antibiotic-Resistant Isolates of *Pseudomonas aeruginosa* and
Enterobacter aerogenes and Methicillin-Resistant *Staphylococcus aureus*.
Appl. Environ. Microbiol. **2012**, *78* (8), 2768-2774.

22. Mu, H.; Tang, J.; Liu, Q.; Sun, C.; Wang, T.; Duan, J., Potent
Antibacterial Nanoparticles against Biofilm and Intracellular Bacteria. *Sci.*
Rep. **2016**, *6*, 18877.

23. Payne, J. N.; Waghwan, H. K.; Connor, M. G.; Hamilton, W.;
Tockstein, S.; Moolani, H.; Chavda, F.; Badwaik, V.; Lawrenz, M. B.;
Dakshinamurthy, R., Novel Synthesis of Kanamycin Conjugated Gold
Nanoparticles with Potent Antibacterial Activity. *Front. Microbiol.* **2016**, *7*,
607.

24. Neu, H. C., Clinical Use of the Quinolones. *Lancet* **1987**, 2 (8571), 1319-1322.
25. Hauser, A. R., *Antibiotic Basics for Clinicians: Choosing the Right Antibacterial Agent*. Wolters Kluwer: Philadelphia, 2007.
26. Fouladgar, M.; Hadjmohammadi, M. R.; Khalilzadeh, M. A.; Biparva, P.; Teymoori, N.; Beitollah, H., Voltammetric Determination of Amoxicillin at the Electrochemical Sensor Ferrocenedicarboxylic Acid Multi Wall Carbon Nanotubes Paste Electrode. *Int. J. Electrochem. Sc.* **2011**, 6 (5), 1355-1366.
27. Simpson, C. A.; Salleng, K. J.; Cliffel, D. E.; Feldheim, D. L., In vivo toxicity, biodistribution, and clearance of glutathione-coated gold nanoparticles. *Nanomед. Nanotechnol.* **2013**, 9 (2), 257-263.
28. Kelly, K. L.; Coronado, E.; Zhao, L. L.; Schatz, G. C., The Optical Properties of Metal Nanoparticles: The Influence of Size, Shape, and Dielectric Environment. *J. Phys. Chem. B* **2003**, 107 (3), 668-677.
29. Gillies, M.; Ranakusuma, A.; Hoffmann, T.; Thorning, S.; McGuire, T.; Glasziou, P.; Del Mar, C., Common harms from amoxicillin: a systematic review and meta-analysis of randomized placebo-controlled trials for any indication. *Can. Med. Assoc. J.* **2015**, 187 (1), E21-E31.
30. Schrag, S. J.; Pena, C.; Fernandez, J.; Sanchez, J.; Gomez, V.; Perez, E.; Feris, J. M.; Besser, R. E., Effect of short-course, high-dose amoxicillin therapy on resistant pneumococcal carriage - A randomized trial. *J. Am. Med. Assoc.* **2001**, 286 (1), 49-56.
31. Smekalova, M.; Aragon, V.; Panacek, A.; Pucek, R.; Zboril, R.; Kvitek, L., Enhanced antibacterial effect of antibiotics in combination with silver nanoparticles against animal pathogens. *Vet. J.* **2016**, 209, 174-179.
32. Huang, X.; El-Sayed, M. A., Gold nanoparticles: Optical properties and implementations in cancer diagnosis and photothermal therapy. *Journal of Advanced Research* **2010**, 1 (1), 13-28.
33. St Denis, T. G.; Huang, L. Y.; Dai, T. H.; Hamblin, M. R., Analysis of the Bacterial Heat Shock Response to Photodynamic Therapy-mediated Oxidative Stress. *Photochem. Photobiol.* **2011**, 87 (3), 707-713.
34. Zhu, Y.; Ramasamy, M.; Yi, D. K., Antibacterial Activity of Ordered Gold Nanorod Arrays. *ACS Appl Mater Inter* **2014**, 6 (17), 15078-15085.
35. Ramasamy, M.; Lee, S. S.; Yi, D. K.; Kim, K., Magnetic, optical gold nanorods for recyclable photothermal ablation of bacteria. *J Mater Chem B* **2014**, 2 (8), 981-988.
36. Leibiger, C.; Kosyakova, N.; Mkrtchyan, H.; Gleib, M.; Trifonov, V.; Liehr, T., First Molecular Cytogenetic High Resolution Characterization of the NIH 3T3 Cell Line by Murine Multicolor Banding. *J. Histochem. Cytochem.* **2013**, 61 (4), 306-312.
37. Amoxicillin, <https://www.drugbank.ca/drugs/DB01060> Access date: July, 2017.
38. Wijesiri, N.; Ozkaya-Ahmadov, T.; Wang, P.; Zhang, J.; Tang, H.; Yu, X.; Ayres, N.; Zhang, P., Photodynamic Inactivation of Multidrug-Resistant Staphylococcus aureus Using Hybrid Photosensitizers Based on Amphiphilic Block Copolymer-Functionalized Gold Nanoparticles. *ACS Omega* **2017**, 2 (9), 5364-5369.
39. Dönmez Güngüneş, Ç.; Şeker, Ş.; Elçin, A. E.; Elçin, Y. M., A comparative study on the in vitro cytotoxic responses of two mammalian cell types to fullerenes, carbon nanotubes and iron oxide nanoparticles. *Drug Chem. Toxicol.* **2017**, 40 (2), 215-227.
40. Aseichev, A. V.; Azizova, O. A.; Beckman, E. M.; Skotnikova, O. I.; Dudnik, L. B.; Shcheglovitova, O. N.; Sergienko, V. I., Effects of Gold Nanoparticles on Erythrocyte Hemolysis. *Bull. Exp. Biol. Med.* **2014**, 156 (4), 495-498.
41. Miao, Y. M.; Li, Y. T.; Zhang, Z. F.; Yan, G. Q.; Bi, Y., "Turn off-on" phosphorescent biosensors for detection of DNA based on quantum dots/acridine orange. *Anal. Biochem.* **2015**, 475, 32-39.
42. Blears, D. J.; Danyluk, S. S., A Nuclear Magnetic Resonance Investigation of Aggregation of Acridine Orange in Aqueous Solution. *J. Am. Chem. Soc.* **1967**, 89 (1), 21-26.
43. Kubota, Y.; Steiner, R. F., Fluorescence Decay and Quantum Yield Characteristics of Acridine-Orange and Proflavine Bound to DNA. *Biophys. Chem.* **1977**, 6 (3), 279-289.
44. Nagata, S., DNA degradation in development and programmed cell death. *Annu. Rev. Immunol.* **2005**, 23, 853-875.
45. Ueki, S.; Konno, Y.; Takeda, M.; Moritoki, Y.; Hirokawa, M.; Matsuwaki, Y.; Honda, K.; Ohta, N.; Yamamoto, S.; Takagi, Y.; Wada, A.; Weller, P. F., Eosinophil extracellular trap cell death-derived DNA traps: Their presence in secretions and functional attributes. *J. Allergy Clin. Immunol.* **2016**, 137 (1), 258-267.
46. Robbins, E.; Marcus, P. I., Dynamics of Acridine Orange-Cell Interaction .1. Interrelationships of Acridine Orange Particles and Cytoplasmic Reddening. *J. Cell Biol.* **1963**, 18 (2), 237-8.
47. Mansour, J. D.; Schram, J. L.; Schulte, T. H., Fluorescent Staining of Intracellular and Extracellular Bacteria in Blood. *J. Clin. Microbiol.* **1984**, 19 (4), 453-456.
48. Frey, T., Nucleic-Acid Dyes for Detection of Apoptosis in Live Cells. *Cytometry* **1995**, 21 (3), 265-274.
49. Longmire, M.; Choyke, P. L.; Kobayashi, H., Clearance properties of nano-sized particles and molecules as imaging agents: considerations and caveats. *Nanomedicine* **2008**, 3 (5), 703-717.
50. Sutariya, V. B.; Pathak, Y., *Biointeractions of Nanomaterials*. CRC Press: 2014.
51. Kumari, A.; Yadav, S. K.; Yadav, S. C., Biodegradable polymeric nanoparticles based drug delivery systems. *Colloids Surf, B* **2010**, 75 (1), 1-18.
52. Hainfeld, J. F.; Slatkin, D. N.; Focella, T. M.; Smilowitz, H. M., Gold nanoparticles: a new X-ray contrast agent. *Br. J. Radiol.* **2006**, 79 (939), 248-253.
53. Hernandez-Sierra, J. F.; Ruiz, F.; Pena, D. C. C.; Martinez-Gutierrez, F.; Martinez, A. E.; Guillen, A. D. P.; Tapia-Perez, H.; Martinez-Castanon, G. A., The antimicrobial sensitivity of Streptococcus mutans to nanoparticles of silver, zinc oxide, and gold. *Nanomед. Nanotechnol.* **2008**, 4 (3), 237-240.
54. Semmler-Behnke, M.; Kreyling, W. G.; Lipka, J.; Fertsch, S.; Wenk, A.; Takenaka, S.; Schmid, G.; Brandau, W., Biodistribution of 1.4- and 18-nm Gold Particles in Rats. *Small* **2008**, 4 (12), 2108-2111.
55. Balasubramanian, S. K.; Jittiwat, J.; Manikandan, J.; Ong, C. N.; Yu, L. E.; Ong, W. Y., Biodistribution of gold nanoparticles and gene expression changes in the liver and spleen after intravenous administration in rats. *Biomaterials* **2010**, 31 (8), 2034-2042.
56. Dikalov, S. I.; Harrison, D. G., Methods for Detection of Mitochondrial and Cellular Reactive Oxygen Species. *Antioxid Redox Sign* **2014**, 20 (2), 372-382.
57. Sigma Cell Proliferation Kit I (MTT) 11465007001. <http://www.sigmaaldrich.com/catalog/product/roche/11465007001?lang=en&C2%AEion=CA> Access date: July, 2017.
58. Choi, J.; Reipa, V.; Hitchins, V. M.; Goering, P. L.; Malinauskas, R. A., Physicochemical Characterization and In Vitro Hemolysis Evaluation of Silver Nanoparticles. *Toxicol. Sci.* **2011**, 123 (1), 133-143.
59. Tomita, G., Fluorescence-Excitation Spectra of Acridine Orange-DNA and -RNA Systems. *Biophysik* **1967**, 4 (1), 23-29.
60. Sayed, M.; Krishnamurthy, B.; Pal, H., Unraveling multiple binding modes of acridine orange to DNA using a multispectroscopic approach. *Phys. Chem. Chem. Phys.* **2016**, 18 (35), 24642-24653.
61. Institute for Laboratory Animal Research (U.S.), & (U.S.), N. A. (2010). Guide for the Care and Use of Laboratory Animals (8th Edition). National Academies Press
62. Parasuraman, S.; Raveendran, R.; Kesavan, R., Blood sample collection in small laboratory animals. *J. Pharmacol. Pharmacother.* **2010**, 1 (2), 87-93.

TOC artwork

